Fracture toughness of high performance concrete subjected to elevated temperatures Part 2 The effects of heating rate, exposure time and cooling rate

Binsheng Zhang[*], Martin Cullen[a] and Tony Kilpatrick[b]

*School of Engineering and Built Environment, Glasgow Caledonian University,
Cowcaddens Road, Glasgow G4 0BA, Scotland, UK*

Abstract. In this study, the fracture toughness K_{IC} of high performance concrete (HPC) was investigated by conducting three-point bending tests on a total of 240 notched beams of 500 mm×100 mm×100 mm subjected to heating temperatures up to 450ºC with exposure times up to 16 hours and various heating and cooling rates. For a heating rate of 3ºC/min, K_{IC} for the hot concrete sustained a monotonic decrease trend with the increasing heating temperature and exposure time, from 1.389 MN/m$^{1.5}$ at room temperature to 0.942 MN/m$^{1.5}$ at 450ºC for 4-hour exposure time, 0.906 MN/m$^{1.5}$ for 8-hour exposure time and 0.866 MN/m$^{1.5}$ for 16-hour exposure time. For the cold concrete, K_{IC} sustained a two-stage decrease trend, dropping slowly with the heating temperature up to 150ºC and then rapidly down to 0.869 MN/m$^{1.5}$ at 450ºC for 4-hour exposure time, 0.812 MN/m$^{1.5}$ for 8-hour exposure time and 0.771 MN/m$^{1.5}$ for 16-hour exposure time. In general, the K_{IC} values for the hot concrete up to 200ºC were larger than those for the cold concrete, and an inverse trend was observed thereafter. The increase in heating rate slightly decreased K_{IC}, and at 450ºC K_{IC} decreased from 0.893 MN/m$^{1.5}$ for 1ºC/min to 0.839 MN/m$^{1.5}$ for 10ºC/min for the hot concrete and from 0.792 MN/m$^{1.5}$ for 1ºC/min to 0.743 MN/m$^{1.5}$ for 10ºC/min for the cold concrete after an exposure time of 16 hours. The increase in cooling rate also slightly decreased K_{IC}, and at 450ºC K_{IC} decreased from 0.771 MN/m$^{1.5}$ for slow cooling to 0.739 MN/m$^{1.5}$ for fast cooling after an exposure time of 16 hours. The fracture energy-based fracture toughness K_{IC}' was also assessed, and similar decrease trends with the heating temperature and exposure time existed for both hot and cold concretes. The relationships of two fracture toughness parameters with the weight loss and the modulus of rapture were also evaluated.

Keywords: HPC; fracture toughness; exposure time; heating rate; cooling rate; weight loss

1. Introduction

High strength concrete and even ultra-high strength concrete has been largely utilised for modern constructions, e.g., tall reinforced concrete buildings, reinforced concrete cooling towers

*Corresponding author, Professor, E-mail: Ben.Zhang@gcu.ac.uk
[a]Senior Lecturer, E-mail: M.N.Cullen@gcu.ac.uk
[b]Senior Lecturer, E-mail: A.R.Kilpatrick@gcu.ac.uk

in thermal power plants, prestressed concrete pressure vessels in nuclear power stations, prestressed concrete silos in chemical factories, long prestressed concrete bridges, marine structures, etc., where concrete needs have ability to sustain elevated temperatures. High strength concrete normally possesses high toughness but also relatively high brittleness, which unavoidably causes concrete to fail suddenly and even explosively at high temperatures and high pressures (Zhang *et al.* 2016). Toughness has been regarded as a fundamental fracture property for assessing the resistance of high performance concrete against cracking and fracture and is a synthetic property. By contrast brittleness is commonly understood to be the tendency for concrete to fracture rapidly before significant deformation occurs. Fracture toughness is a widely used parameter for fracture analysis. The information about toughness of high strength high performance concrete under highly elevated temperatures is very limited but is much required for manufacturing high strength high performance concrete materials, designing modern concrete structures, conducting structural analysis and simulations under various loading and environmental conditions, and assessing post-fire safety of reinforced and prestressed high strength concrete structures.

Kaplan first measured the fracture toughness and strain energy release rate of concrete in the early 1960s (Kaplan 1961). Since then, much theoretical and experimental work has been done to assess whether linear elastic fracture mechanics (LEFM) could be directly applied to concrete materials. During loading, concrete shows non-linearity before the peak load is reached. The stable crack growth, normally termed as the fracture process zone, occurs due to micro cracks in the mortar and cracks at cement paste-aggregate interface, or crack arresting, kinking and linking between aggregate particles, or a macro crack, which makes the measured fracture toughness be geometrically dependent. To accurately determine the fracture toughness of concrete, the stable crack growth has to be added to the initial notch depth and the effective crack length is adopted to make the obtained fracture toughness be a true material property which is fully geometrically independent. Hillerborg used the fictitious crack model to define the stable propagation zone of the crack (Hillerborg *et al.* 1976). Bažant *et al.* used the size effect model and the crack band model to determine *R*-curve parameters, crack band width, strain softening modulus, etc. (Bažant and Oh 1983, Bažant 1984, Bažant *et al.* 1986, Gettu *et al.* 1990). Karihaloo and Nallathambi extensively investigated the effects of crack size, water/cement ratio and coarse aggregate texture on the fracture toughness of concrete and proposed the effective crack model based on massive test data for calculating the fracture toughness, and their empirical formulae are very convenient to use (Nallathambi *et al.* 1984, Karihaloo and Nallathambi 1989). Shah (1990) proposed the two-parameter fracture model to determine the effective crack length. RILEM (1990a, 1990b) proposed the drafts for determining the fracture toughness K_{IC} and the critical crack tip opening displacement $CTOD_c$ by using either Shah's two-parameter model (Shah 1990) or Bažant's size effect model (Bažant *et al.* 1986). Direct tension (Phillips and Zhang 1993) and splitting tension tests (Ince 2010) were tried to obtain stable fracture toughness of concrete. Xu and Reinhardt (1999a, 1999b, 1999c, 2000) proposed the double-*K* fracture model to simulate the fracture of concrete including the initial fracture toughness K_{IC}^{ini} and the unstable fracture toughness K_{IC}^{un} measured on the compact tension, wedge splitting and three-point bending concrete specimens. Recently, Wu and Dong extensively investigated the fracture process zones on concrete and rock-concrete interface, experimentally and numerically, for accurately calculating the fracture toughness parameters (Wu *et al.* 2011, 2013, Dong *et al.* 2013, 2016).

Prokoski (1995) was the earliest researcher who measured the fracture toughness of ordinary

and refractory concretes exposed up to 1300°C at 28 days on the concrete beams under three-point bending. However, an exposure time of 2 hours at high temperatures may not be long enough for obtaining a uniform temperature within the concrete specimen and very large thermal and hygric gradients would still exist. In his calculations, he only used the initial crack length and ignored the stable propagation of the pre-crack, which led to the K_{IC} values to be geometrically dependent. Hamoush and his colleagues (1998) measured the residual fracture toughness of normal strength crushed limestone concrete on forty-five notched beams under three-point bending by considering a process zone at the peak load and found that K_{IC} monotonically decreased with increasing temperatures. The maximum heating temperature in his study was only 300ºC so the application of his test results is limited. Meanwhile, neither of them considered the effect of self-weight of the beam even though this effect became more significant when the concrete beams were tested after having sustained high temperatures, which would lead to the test data to be less accurate. Zhang and Bićanić (2002) investigated the classic fracture toughness, K_{IC}, and the fracture energy related fracture toughness, K_{IC}', for assessing the residual fracture toughness of heated normal- and high-strength concrete. The effects of heating temperature, exposure time and curing age were experimentally investigated on eighty-seven notched concrete beams that had been heated up to 600ºC over various exposure times and cooled down to the room temperature. Higher heating temperature over 200ºC generally decreased fracture toughness but below 200ºC some strengthening and toughening effect was observed. Similar phenomenon was found for longer exposure time as well but such effect was more significant at the early exposure stage under 12 hours. Longer curing age only led to slightly larger toughness in the first 28 days and became little influential thereafter. Yu and Lu (2014) determined the residual double-K fracture toughness of post-fire concrete using analytical and weight function method.

So far, information about the fracture toughness of concrete exposed to high temperatures is very limited even though K_{IC} can be used to assess the resistance of concrete against cracking and failure at high temperatures. The determination of the fracture process zone size will be very important for accurately calculating the fracture toughness at high temperatures. Hence, more work needs to be done to further study the effect of varied heating scenarios on the fracture toughness of concrete at high temperatures. The effect of moisture migration on the fracture toughness also needs to be further investigated.

In this study, the test programme was divided into several series. Each series was specially designed to target one parameter which would largely influence the fracture toughness and other fracture properties of high performance concrete, including the heating temperature T_m, the testing conditions (hot and cold), the heating rate $\dot{T}^+$, the cooling rate $\dot{T}^-$ (cooling methods) and the exposure time t_h at the designated temperature. In the previous paper (Zhang *et al.* 2014), the test results regarding the effects of the heating temperature T_m and the testing conditions (hot or cold) on the fracture toughness and other properties of the concrete have been reported. In this paper, the test results regarding the effects of the exposure time t_h, the heating rate $\dot{T}^+$ and the cooling rate $\dot{T}^-$, together with T_m on the fracture toughness and other properties of the concrete are presented. Those effects were also investigated by conducting three-point bending tests on the notched beams of high performance concrete in a furnace. Beside the fracture toughness K_{IC}, the compressive strength f_{cu}, the splitting tensile strength f_t', the modulus of rupture f_r, the fracture toughness G_F and the Young's modulus E were also studied. K_{IC}, G_F and f_r were measured under both hot and cold conditions, whereas other properties were measured after cooling (residual). The weight loss ω was continuously measured while the concrete was heated and could be used to further study
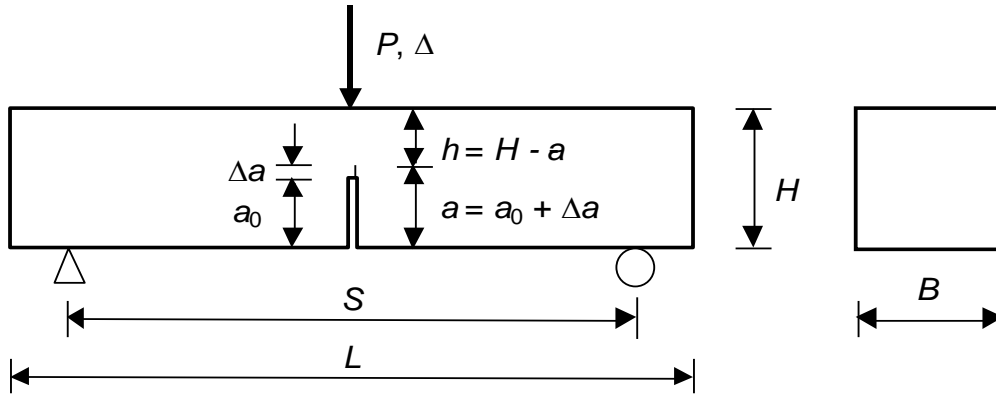
Fig. 1 Dimensions of a single edge notched beam in three-point bending

its effect on the fracture behaviour of the concrete during heating. Thus, the relationships of K_{IC} and other fracture properties with T_m, t_h, $\dot{T}^+$, $\dot{T}^-$ and ω could be synthetically established.

2. Fracture mechanics and fracture toughness

2.1 Fracture toughness of concrete

In the linear fracture mechanics (*LEFM*), the fracture toughness or the critical stress intensity factor for mode I, K_{IC}, is generally calculated from

$$K_{IC} = \sigma_N \sqrt{a}\, F(\alpha) \tag{1}$$

where
σ_N is the nominal applied stress,
a is the effective crack length and $a = a_0 + \Delta a$,
a_0 is the initial notch depth,
Δa is the crack propagation at peak load, also regarded as the size of the process or crack zone,
α is the effective notch-depth ratio and $\alpha = a/H$,
H is the specimen depth,
$F(\alpha)$ is a geometric function.

Fig. 1 shows the arrangement of the three-point bending test on a notched concrete beam for determining K_{IC}. Thus, σ_N in Eq. (1) is equal to the modulus of rupture of the corresponding un-notched beam by considering the self-weight of the beam as

$$\sigma_N = \frac{6\,M}{B\,H^2} = \frac{1.5\,(P_u + P_0)\,S}{B\,H^2} = \frac{1.5\,[P_u + 0.5\,m\,g\,(L/S)\,(2 - L/S)]\,S}{B\,H^2} \tag{2}$$

where
B is the width of the beam,
L is the full length of the beam,

S is the effective span,

M is the maximum moment at the middle span, given by $M = (P_u + P_0) S/4$,

P_u is the maximum load at peak,

P_0 is the equivalent load due to the self-weight of the beam and $P_0 = 0.5 \, m \, g \, (L/S) \, (2 - L/S)$,

m is the mass of the beam between the supports and is calculated as $m = m_0 \, (S/L)$,

m_0 is the total mass of the beam,

g is the acceleration due to gravity and $g = 9.81 \text{ m/s}^2$.

Here the ligament height h is equal to $H - a$. At high temperatures, the self-weight of the beam, m, is replaced by the actual mass m' as

$$m' = m \, (1 - \omega) \tag{3}$$

where ω is the percentage weight loss during heating, greatly dependent on heating scenarios. For $S/H = 4$, the geometric function $F(\alpha)$ can be expressed as (Karihaloo and Nallathambi 1989, RILEM 1990a)

$$F(\alpha) = \frac{1.99 - \alpha \, (1 - \alpha) \, (2.15 - 3.93 \, \alpha + 2.70 \, \alpha^2)}{(1 + 2 \, \alpha) \, (1 - \alpha)^{3/2}} \tag{4}$$

From this model, the effective crack length a can be obtained from

$$\frac{a}{H} = \gamma_1 \left(\frac{\sigma_N}{E}\right)^{\gamma_2} \left(\frac{a_0}{H}\right)^{\gamma_3} \left(1 + \frac{d}{H}\right)^{\gamma_4} \tag{5}$$

where

d is the maximum aggregate size used in the concrete mix,

E is the Young's modulus of concrete,

γ_1 to γ_4 are constants and can be obtained from the best fit method on test data.

When E is obtained from separate tests, $\gamma_1 = 0.198$, $\gamma_2 = -0.131$, $\gamma_3 = 0.394$ and $\gamma_4 = 0.600$ (Karihaloo and Nallathambi 1989).

In the process for determining K_{IC}, σ_N is calculated first using Eq. (2), then followed by determining $\alpha = a/H$ using Eq. (5) and $F(\alpha)$ using Eq. (4), and finally calculating K_{IC} using Eq. (1). The modulus of rupture f_r of the notched beam can be determined as

$$f_r = \frac{6 \, M}{B \, (H - a_0)^2} = \frac{1.5 \, (P_u + P_0) \, S}{B \, (H - a_0)^2} = \frac{1.5 \, [P_u + 0.5 \, m \, g \, (L/S) \, (2 - L/S)] \, S}{B \, (H - a_0)^2} \tag{6}$$

In this study, $a_0/H = 0.5$ so $f_r = 4\sigma_N$.

The fracture energy, G_F, defined as the total energy dissipated over a unit area of the cracked ligament, was obtained on the basis of the work done by the force (the area under a load-displacement curve (P–Δ curve) in three-point bending on a centrally notched beam) associated with the gravitational work done by the self-weight of the beam. G_F was calculated based on the following formula

$$G_F = \frac{\int_0^{\Delta_0} P(\Delta) \, d\Delta + m' g \, (L/S) \, (2 - L/S) \, \Delta_0}{B \, (H - a_0)} \tag{7}$$

Here, Δ_0 is the ultimate displacement when the beam is broken.

Binsheng Zhang, Martin Cullen and Tony Kilpatrick

Table 1 Complete test series and residual material properties of HPC for various heating scenarios

$\dot{T}^+$ (ºC/min)	T_m (ºC)	t_h (hour)	$\dot{T}^-$	Number of Specimens*	f_{cu} (MPa)	f_t' (MPa)	E (GPa)	ω_u (%)
/	20	/	/	5	67.1	4.47	35.64	0.00
1	150	16	Slow	7 (4 + 3)	63.4	3.81	27.19	4.47
	300			7 (4 + 3)	62.0	3.26	17.85	5.87
	450			7 (4 + 3)	55.3	2.64	10.65	6.65
3	150	4	Slow	6 (3 + 3)	57.6	3.70	32.63	3.31
	200			7 (4 + 3)	66.7	3.80	27.95	4.28
	250			7 (4 + 3)	66.2	3.70	24.02	5.30
	300			7 (4 + 3)	64.4	3.58	20.02	5.79
	350			7 (4 + 3)	62.2	3.38	16.93	6.12
	400			7 (4 + 3)	59.3	3.19	13.91	6.43
	450			9 (2 + 3 + 4)	56.3	3.02	10.93	6.59
	150	8	Slow	6 (3 + 3)	60.5	3.63	29.96	3.93
	200			7 (4 + 3)	65.0	3.65	25.98	4.92
	250			7 (4 + 3)	64.2	3.51	22.37	5.42
	300			7 (4 + 3)	62.3	3.32	18.23	5.92
	350			7 (4 + 3)	60.1	3.09	15.14	6.21
	400			6 (3 + 3)	57.6	2.90	12.78	6.53
	450			7 (4 + 3)	54.8	2.70	10.59	6.62
	105	16	Slow	7 (4 + 3)	55.2	3.40	29.82	2.46
	150			10 (7 + 3)	61.9	3.61	27.05	4.59
	200			10 (7 + 3)	63.7	3.55	23.80	5.16
	250			10 (7 + 3)	62.9	3.31	21.12	5.58
	300			10 (7 + 3)	60.9	3.11	17.57	5.97
	350			10 (7 + 3)	58.8	2.91	14.75	6.28
	400			9 (6 + 3)	56.4	2.71	12.53	6.62
	450			9 (2 + 3 + 4)	53.8	2.48	9.99	6.76
	150	16	Fast	3 (*4* + 3)	61.8	3.30	26.24	4.64
	200			3 (*4* + 3)	62.9	3.46	23.29	5.28
	250			3 (*4* + 3)	61.9	3.22	20.94	5.65
	300			3 (*4* + 3)	59.5	3.01	17.45	6.08
	350			3 (*4* + 3)	57.4	2.79	13.81	6.39
	400			3 (*4* + 3)	54.9	2.58	12.18	6.70
	450			3 (2 + 3 + *4*)	51.8	2.35	9.90	6.86
10	150	16	Slow	7 (4 + 3)	61.2	3.51	26.86	4.64
	300			7 (4 + 3)	60.3	3.01	17.44	6.09
	450			7 (4 + 3)	53.2	2.38	9.16	6.85
Total				240				

*In Table 1, the first numbers in the brackets represent the beams tested under hot conditions; the second numbers represent the beams tested after cooling; the third numbers represent the beams sustaining spalling; the numbers in italic represent the beams accounted duplicately

The fracture toughness can also be calculated using the fracture energy G_F and the Young's modulus E in LEFM, termed as K_{IC}' as follows

$$K_{IC}' = \sqrt{G_F\, E} \tag{8}$$

As indicated in the previous paper (Zhang *et al.* 2014), the classic fracture toughness K_{IC} is obtained based on the ultimate load on the ascending branch of a load-displacement curve, including linear loading part and hardening part. It can be used to reflect the resistance of concrete against cracking. The fracture toughness related to fracture energy, K_{IC}', can represent the behaviour of concrete at the complete loading process including linear, hardening and softening parts, and its magnitude can be expected to be larger than K_{IC} but its physical meaning can be clearer and more rational.

3. Experimental

3.1 Concrete specimens

For the complete test series, eight heating temperatures were adopted as T_m = 105ºC, 150ºC, 200ºC, 250ºC, 300ºC, 350ºC, 400ºC and 450ºC, respectively, together with three heating rates $\dot{T}^+$ = $(dT/dt)^+$ = 1ºC/min, 3ºC/min and 10ºC/min. The exposure time at a designated temperature was fixed at t_h = 4 hours, 8 hours and 16 hours, respectively. Cooling was conducted by leaving the furnace either fully closed or fully open to obtain slow and fast cooling conditions. A total of 240 beams were tested with at least three beams for each scenario, and 140 prisms were tested only for obtaining the residual Young's modulus. As bench marks, five beams and three prisms were tested at 20ºC. Table 1 lists the arrangement of the complete test series with the heating scenarios as heating rate, heating temperature, exposure time, cooling rate and testing conditions (hot or cold).

The primary fracture parameters measured under both hot and cold conditions were the fracture energy G_F, fracture toughness K_{IC} and the modulus of rupture f_r. The residual material properties measured were the compressive strength f_{cu}, splitting tensile strength f_t', Young's modulus E and concrete density ρ. The weight loss ω was continuously measured when the concrete was heated and could be used to further study its effect on the fracture behaviour of concrete during heating. Part of the test data for the above mentioned parameters for different heating scenarios have been reported in previous publications (Zhang and Bićanić 2006, Zhang 2011, Zhang *et al.* 2014).

Table 2 Concrete mix design in weight

Contents	42.5N OPC	PFA	Quartz sand	10 mm dolerite	20 mm dolerite	Water	Pozzolith 300 N Plasticizer	Slump (mm)
Weight ratio	1	0.33	2.45	1.39	2.78	0.56	0.006	
Quantities (kg/m³)	300	99	735	417	834	168	1.8	125

Notched concrete beams of 500 mm × 100 mm × 100 mm, with a 400 mm effective span and a 50 mm notch depth, were loaded under three-point bending for determining G_F, K_{IC} and f_r. Notches were prepared using a diamond saw before being heated. Concrete prisms of 200 mm × 100 mm × 100 mm were cast for determining the residual E, three for each scenario. To effectively utilise the heated concrete, 100 mm cubes were cut from the broken beams for obtaining f_{cu} and f_t'.

The test age was at least 90 days to allow full hydration, giving f_{cu} = 67.1 MPa, f_t' = 4.47 MPa, E = 35.64 GPa and ρ = 2463 kg/m^3. The residual properties of the HPC for the complete series were presented in Table 1, including f_{cu}, f_t', E and the final weight loss ω_u. The concrete mix design is listed in Table 2.

3.2 Heating furnace and testing facility

A specially designed program-controlled three-zone VTS furnace (600 ± 5ºC) had two identical halves with inner dimensions of 600 mm × 600 mm × 800 mm. It was built within the 2000 kN LOS universal testing machine to allow the tests to be done at high temperatures. Fans were used to circulate the air in the furnace for heating the concrete uniformly and cooling the loading pieces.

A high yield strength steel loading piece was designed to allow two beams to be tested while being hot in one heating batch. The bottom block was connected to the lower actuator of the machine. A plate on the block could slide against it after being slightly raised by using two lifting bars. Prior to heating, two beams were put on the loading piece symmetrically in the furnace. When the heating process was completed, one beam was lifted to the centre of the machine and then tested. The second beam could then be lifted to the centre for testing. High yield strength steel was also used for the top piece which was connected to the upper actuator. According to the requirement by RILEM, a roller bearing was used for one support for each beam and a ball bearing for the other. The heating furnace within the testing machine and the loading pieces with the twin concrete specimens have been illustrated in the previous publication (Zhang *et al.* 2014).

A 10 kN high temperature load cell, located outside the furnace, was inserted between the top piece and top actuator for load measurement due to its temperature working limit of 180ºC and continuously cooled during the heating-testing process so that the actual temperature in the load cell was below 50°C. The displacement of the machine was automatically recorded using a built-in displacement transducer. Four LIN high temperature linear voltage displacement transducers (LVDTs) with a temperature working limit of 600°C were also used for monitoring the creep of the concrete during heating, two for each beam.

Three-point bending tests were conducted at high temperatures and after cooling at a displacement rate of 1.25×10^{-3} mm/s. The load and displacements were recorded using a data logger at a rate of two sets per second. Each three-point bending test took 10 to 15 minutes.

To monitor the temperature developments in the concrete, N-type thermocouples were embedded in the beams for three-point bending tests. Two positions were chosen for each beam: 50 mm close to the edge (side hole) and 50 mm away from the centre (middle hole) to avoid disturbing the notched mid-section. The 50 mm deep holes were drilled before the beams were heated. The temperatures from the thermocouples in the three heating zones and from the master thermocouple of the furnace were recorded.

The DNG7229 3000 kN machine was used to measure f_{cu} and f_t' on at least six cubes for each scenario. The Testwell TE6000 3000 kN servo testing machine was used to test E on four prisms. All the test results of the fracture characteristics of the concrete for complete test series with various heating scenarios and test conditions (hot and cold conditions) are listed in Table 3,

Table 3 Fracture properties of the HPC under hot and cold conditions for various heating scenarios*

$\dot{T}^{+}$ (°C/min)	T_{m} (°C)	t_{h} (hour)	$\dot{T}^{-}$	f_{r} (MPa) Hot	Cold	G_{F} (N/m) Hot	Cold	K_{IC} (MN/m$^{1.5}$) Hot	Cold	K_{IC}' (MN/m$^{1.5}$) Hot	Cold
/	20	/	/	6.35		228.2		1.389		2.845	
1	150	16	Slow	6.20	6.75	199.8	265.3	1.255	1.331	2.330	2.684
	300			6.06	5.47	264.6	328.6	1.092	1.015	2.170	2.415
	450			5.53	4.71	313.2	267.1	0.893	0.792	1.826	1.686
	150	4	Slow	4.81	5.92	248.3	226.0	1.124	1.289	2.836	2.714
	200			5.46	6.47	236.6	240.2	1.161	1.303	2.564	2.587
	250			6.11	6.29	229.5	260.1	1.196	1.221	2.342	2.491
	300			6.42	6.07	234.4	286.5	1.175	1.129	2.157	2.375
	350			6.22	5.73	244.9	299.6	1.097	1.033	2.036	2.251
	400			6.02	5.48	254.3	302.5	1.018	0.949	1.881	2.051
	450			5.88	5.29	264.3	280.7	0.942	0.869	1.690	1.751
	150	8	Slow	5.37	6.22	217.0	243.1	1.173	1.297	2.527	2.698
	200			5.85	6.66	231.2	261.8	1.189	1.301	2.445	2.607
	250			6.19	6.03	241.9	284.1	1.182	1.161	2.321	2.514
	300			6.18	5.72	247.3	299.0	1.114	1.054	2.122	2.331
	350			6.01	5.36	262.1	306.9	1.039	0.956	1.988	2.138
	400			5.82	5.12	278.3	294.4	0.972	0.884	1.880	1.940
	450			5.64	4.88	292.5	269.2	0.906	0.812	1.760	1.688
3	105	16	Slow	4.89	6.43	205.6	223.0	1.101	1.323	2.471	2.574
	150			6.13	6.65	191.5	258.9	1.243	1.316	2.272	2.645
	200			6.33	6.35	212.2	286.4	1.223	1.227	2.247	2.607
	250			6.20	5.92	236.3	310.7	1.164	1.126	2.233	2.558
	300			6.01	5.37	258.6	323.7	1.081	0.996	2.122	2.384
	350			5.81	5.13	273.7	310.1	1.006	0.919	2.007	2.138
	400			5.61	4.87	289.9	280.7	0.939	0.847	1.903	1.869
	450			5.41	4.65	303.2	253.4	0.866	0.771	1.737	1.584
	150	16	Fast	*6.13*	6.41	*191.5*	226.6	*1.243*	1.270	*2.272*	2.438
	200			*6.33*	6.15	*212.2*	247.3	*1.223*	1.191	*2.247*	2.399
	250			*6.20*	5.77	*236.3*	279.1	*1.164*	1.103	*2.233*	2.415
	300			*6.01*	5.21	*258.6*	299.2	*1.081*	0.973	*2.122*	2.284
	350			*5.81*	4.93	*273.7*	289.4	*1.006*	0.877	*2.007*	1.997
	400			*5.61*	4.65	*289.9*	271.6	*0.939*	0.813	*1.903*	1.818
	450			*5.41*	4.40	*303.2*	246.4	*0.866*	0.739	*1.737*	1.561
10	150	16	Slow	6.05	6.57	184.6	253.9	1.229	1.301	2.225	2.610
	300			5.91	5.30	252.4	316.9	1.066	0.985	2.096	2.345
	450			5.34	4.55	293.7	241.9	0.839	0.743	1.631	1.485

*The test results in italic under hot conditions represent duplicated ones

including f_r, G_F, K_{IC} and K_{IC}'. At room temperature, $f_r = 6.35$ MPa, $G_F = 228.2$ N/m, $K_{IC} = 1.389$ MN/m$^{1.5}$ and $K_{IC}' = 2.845$ MN/m$^{1.5}$.

3.3 Weight loss measurement

To continuously monitor the moisture migration during heating, exposure, testing and cooling, two steel cradles were made for hanging concrete beams and prisms, each connected to a VC8000 high precision load cell of 25 kg $\pm$ 10 g, fixed outside the furnace. During heating, exposure and cooling, the weight changes were recorded every 5 seconds. During testing, the weight changes were recorded together with the load and displacements at a rate of two sets per second. The values of the final weight loss after the cooling-down stage are also included in Table 1.

4. Fracture toughnesses K_{IC} and K_{IC}' versus heating temperature T_m for various heating rates, exposure times and cooling methods

4.1 Summary of the previous study

The effects of the heating temperature, testing conditions (hot and cold) and weight loss on the fracture toughness and other mechanical properties of the high performance concrete at high temperatures up to 450ºC and a heating rate $\dot{T}^+ = 3$ºC/min were reported in the previous publication (Zhang *et al.* 2014). The main findings are summarised as follows.

K_{IC} for the hot concrete sustained a monotonic decrease tendency with T_m, with a sudden drop at 105ºC due to high vapour pressures within the concrete pores. For the cold concrete, K_{IC} sustained a two-stage decrease trend, dropping slowly with T_m up to 150ºC and rapidly thereafter. When $T_m \leq 200$ºC, K_{IC} for the hot concrete was smaller than that for the cold concrete, and a reverse trend occurred for higher heating temperatures.

K_{IC}' was twice as large as K_{IC} for all heating temperatures. For both hot and cold concretes, K_{IC}' sustained a decrease-hold-decrease tendency with T_m. For most heating temperatures, K_{IC}' for the hot concrete was always smaller than that for the cold concrete except for $T_m \geq 400$ºC.

For the hot concrete, K_{IC} sustained a decrease-recovery-decrease tendency with the final weight loss ω_u. In the first two stages, K_{IC} only slightly decreased with ω_u until 150ºC and then dropped rapidly. K_{IC} for the cold concrete clearly followed a two-stage decrease trends, dropping slowly with ω_u first and then rapidly after 150ºC.

For the hot concrete, K_{IC}' sustained a two-stage decrease tendency with ω_u. K_{IC}' first slowly decreased with ω_u until 250ºC. At the second stage, K_{IC}' continuously but quickly decreased with ω_u. For the cold concrete, K_{IC}' sustained a three-stage decrease-hold-decrease tendency with ω_u. It slightly decreased with ω_u until 105ºC and then was almost unchanged until 250ºC. Thereafter K_{IC}' rapidly decreased with ω_u.

4.2 K_{IC} and K_{IC}' versus T_m for various $\dot{T}^+$

Fig. 2 shows K_{IC} for various heating temperatures and testing conditions over an exposure time $t_h = 16$ hours and slow cooling at different heating rates. In general, K_{IC} decreased with the increasing hearing temperature. Also a higher heating rate slightly decreased K_{IC} for both hot and cold concretes because it would cause larger damage to the concrete.
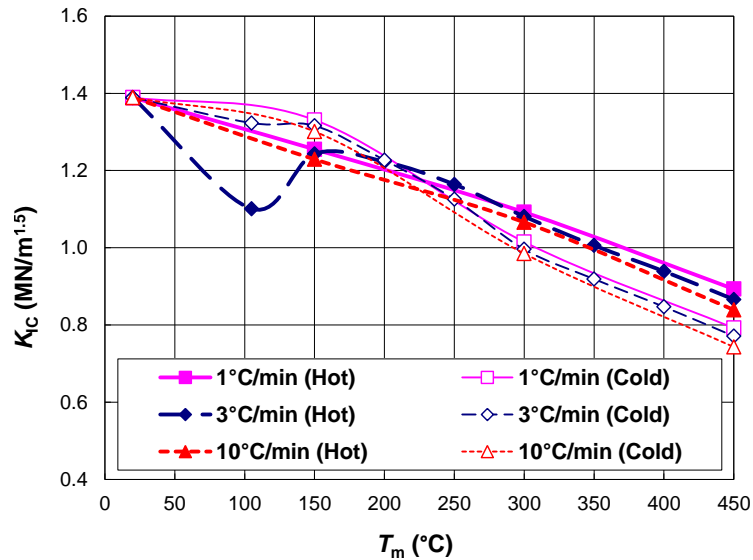
Fig. 2 K_{IC} versus T_{m} for different testing conditions at different heating rates

For the hot concrete, K_{IC} sustained a decrease-recovery-decrease trend but generally followed a decreasing tendency with the increasing T_{m} for all three heating rates. At T_{m} = 150ºC, K_{IC} decreased from 1.389 MN/m$^{1.5}$ at 20ºC to 1.255 MN/m$^{1.5}$ for $\dot{T}^{+}$ = 1°C/min, 1.243 MN/m$^{1.5}$ for $\dot{T}^{+}$ = 3°C/min and 1.229 MN/m$^{1.5}$ for $\dot{T}^{+}$ = 10°C/min, with net drops of 10%, 11% and 12%, respectively. At T_{m} = 300ºC, K_{IC} decreased further to 1.092 MN/m$^{1.5}$ for $\dot{T}^{+}$ = 1°C/min, 1.081 MN/m$^{1.5}$ for $\dot{T}^{+}$ = 3°C/min and 1.066 MN/m$^{1.5}$ for $\dot{T}^{+}$ = 10°C/min, with net drops of 21%, 22% and 23%, respectively. At T_{m} = 450ºC, K_{IC} would finally decrease to 0.893 MN/m$^{1.5}$ for $\dot{T}^{+}$ = 1°C/min, 0.866 MN/m$^{1.5}$ for $\dot{T}^{+}$ = 3°C/min and 0.839 MN/m$^{1.5}$ for $\dot{T}^{+}$ = 10°C/min, with final net drops of 36%, 38% and 40%, respectively. The caused differences in K_{IC} due to the changes in heating rate increased from 1°C/min to 10°C/min varied only between 2% to 4%, which are not significant.

For the cold concrete, K_{IC} sustained a slow decrease up to 150°C and then fast decrease trend with the increasing T_{m} for all three heating rates. At T_{m} = 150°C, K_{IC} decreased from 1.389 MN/m$^{1.5}$ at 20ºC to 1.331 MN/m$^{1.5}$ for $\dot{T}^{+}$ = 1°C/min, 1.316 MN/m$^{1.5}$ for $\dot{T}^{+}$ = 3°C/min and 1.301 MN/m$^{1.5}$ for $\dot{T}^{+}$ = 10°C/min, with net drops of 4%, 5% and 6%, respectively. At T_{m} = 300ºC, K_{IC} decreased further to 1.015 MN/m$^{1.5}$ for $\dot{T}^{+}$ = 1°C/min, 0.996 MN/m$^{1.5}$ for $\dot{T}^{+}$ = 3°C/min and 0.985 MN/m$^{1.5}$ for $\dot{T}^{+}$ = 10°C/min, with net drops of 27%, 28% and 29%, respectively. At T_{m} = 450ºC, K_{IC} would finally decrease to 0.792 MN/m$^{1.5}$ for $\dot{T}^{+}$ = 1°C/min, 0.771 MN/m$^{1.5}$ for $\dot{T}^{+}$ = 3°C/min and 0.743 MN/m$^{1.5}$ for $\dot{T}^{+}$ = 10°C/min, with final net drops of 43%, 45% and 47%, respectively. The caused differences in K_{IC} due to the changes in the heating rate increased from 1°C/min to 10°C/min varied only between 2% to 4%, which are still not significant.

Fig. 2 also shows that for $T_{\text{m}} \leq 200$ºC, the values of K_{IC} for the hot concrete were smaller than those for the cold concrete at all three heating rates. At this stage, the high vapour pressure under hot conditions could not efficiently evaporate so as to significantly reduce the fracture toughness
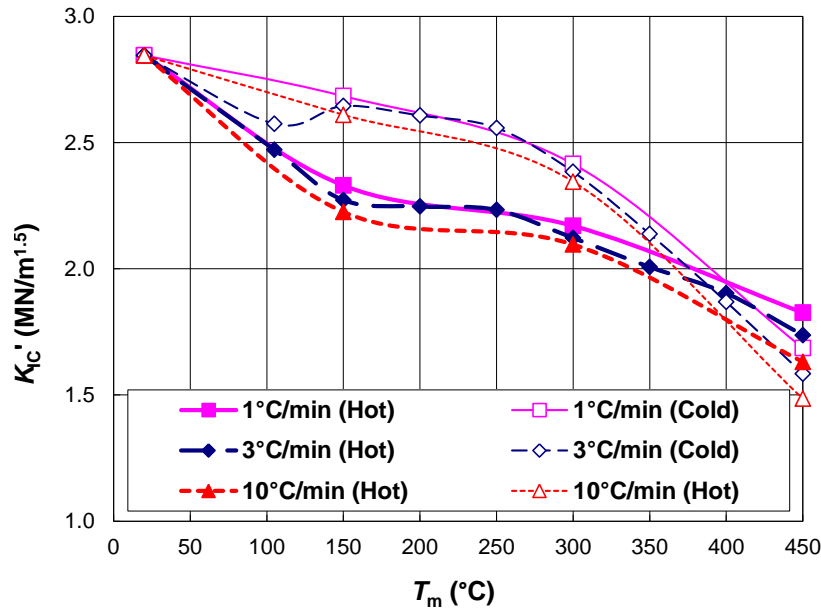
Fig. 3 K_{IC}' versus T_m for different testing conditions at different heating rates

of the concrete. The cooling process eliminated the vapour pressure and did not damage the concrete. For heating temperatures over 200ºC, the values of K_{IC} for the hot concrete were larger than those for the cold concrete. At this stage, there were no longer high vapour pressures within the concrete because micro cracks had already formed. However, cooling would cause more micro cracks and further damage the concrete. Thus, even smaller fracture toughness would be expected.

Fig. 3 shows K_{IC}' for various heating temperatures and testing conditions at different heating rates. K_{IC}' has similar decreasing trends with the hearing temperature and heating rate to K_{IC}. It can be seen that the values of K_{IC}' were twice as large as the values of K_{IC} for all heating temperatures, heating rates and testing conditions. This is because K_{IC} is an instantaneous parameter and represents the cracking resistance at the peak load, while K_{IC}' is a more synthetic process parameter and represents the resistance over the whole fracture process.

For the hot concrete, K_{IC}' sustained a decrease-hold-decrease tendency but generally followed a decrease tendency with increasing T_m for all three heating rates. At $T_m = 150$ºC, K_{IC}' decreased from 2.845 MN/m$^{1.5}$ at 20ºC to 2.330 MN/m$^{1.5}$ for $\dot{T}^+ = 1$°C/min, 2.272 MN/m$^{1.5}$ for $\dot{T}^+ = 3$°C/min and 2.225 MN/m$^{1.5}$ for $\dot{T}^+ = 10$°C/min, with net drops of 18%, 20% and 22%, respectively. At $T_m = 300$ºC, K_{IC}' decreased further to 2.170 MN/m$^{1.5}$ for $\dot{T}^+ = 1$°C/min, 2.122 MN/m$^{1.5}$ for $\dot{T}^+ = 3$°C/min and 2.096 MN/m$^{1.5}$ for $\dot{T}^+ = 10$°C/min, with net drops of 24%, 25% and 26%, respectively. At $T_m = 450$ºC, K_{IC}' would finally decrease to 1.826 MN/m$^{1.5}$ for $\dot{T}^+ = 1$°C/min, 1.737 MN/m$^{1.5}$ for $\dot{T}^+ = 3$°C/min and 1.631 MN/m$^{1.5}$ for $\dot{T}^+ = 10$°C/min, with final net drops of 36%, 39% and 43%, respectively. The caused differences in K_{IC}' due to the changes in the heating rate increased from 1°C/min to 10°C/min varied only between 3% to 7%, which are slightly larger than those for K_{IC}.

For the cold concrete, K_{IC} sustained a slow decrease up to 300°C and then a fast decrease trend with the increasing T_m for all three heating rates. At $T_m = 150$ºC, K_{IC}' decreased from 2.845

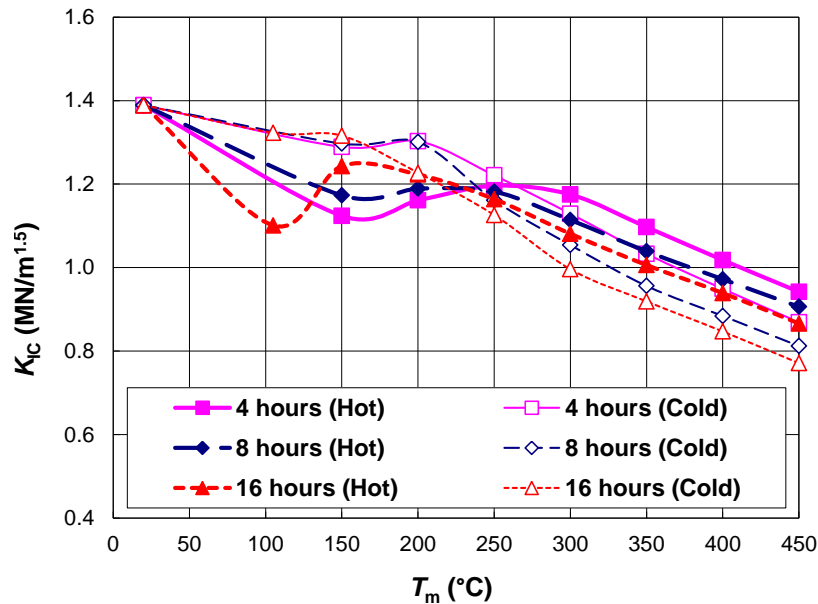Fig. 4 K_{IC} versus T_m for different testing conditions and exposure times

MN/m$^{1.5}$ at 20°C to 2.684 MN/m$^{1.5}$ for $\dot{T}^+ = 1$°C/min, 2.645 MN/m$^{1.5}$ for $\dot{T}^+ = 3$°C/min and 2.610 MN/m$^{1.5}$ for $\dot{T}^+ = 10$°C/min, with net drops of 6%, 7% and 8%, respectively. At $T_m = 300$°C, K_{IC}' decreased further to 2.415 MN/m$^{1.5}$ for $\dot{T}^+ = 1$°C/min, 2.384 MN/m$^{1.5}$ for $\dot{T}^+ = 3$°C/min and 2.345 MN/m$^{1.5}$ for $\dot{T}^+ = 10$°C/min, with net drops of 15%, 16% and 18%, respectively. At $T_m = 450$°C, K_{IC}' would finally decrease to 1.686 MN/m$^{1.5}$ for $\dot{T}^+ = 1$°C/min, 1.584 MN/m$^{1.5}$ for $\dot{T}^+ = 3$°C/min and 1.485 MN/m$^{1.5}$ for $\dot{T}^+ = 10$°C/min, with final net drops of 41%, 44% and 48%, respectively. The caused differences in K_{IC}' due to the changes in the heating rate increased from 1°C/min to 10°C/min varied only between 3% to 7%, which are slightly larger than those for K_{IC} but still relatively small.

For most heating temperatures, the values of K_{IC}' for the hot concrete were always smaller than those for the cold concrete except for $T_m \geq 400$°C.

4.3 K_{IC} and K_{IC}' versus T_m for various t_h

Fig. 4 shows K_{IC} at various heating temperatures over three exposure times, i.e., $t_h = 4$, 8 and 16 hours for $\dot{T}^+ = 3$°C/min and slow cooling. In general, K_{IC} decreased with the increasing hearing temperature and exposure time for both hot and cold concretes because a longer exposure time at higher heating temperatures would cause larger damage to the concrete.

For the hot concrete at lower heating temperatures for three exposure times, K_{IC} had different trends from those at higher temperatures. For heating temperatures up to 250°C, K_{IC} sustained a quick decrease-recovery process. At $T_m = 150$°C, K_{IC} decreased from 1.389 MN/m$^{1.5}$ before heating ($t_h = 0$) to 1.124 MN/m$^{1.5}$ for $t_h = 4$ hours and then started to recover to 1.173 MN/m$^{1.5}$ for $t_h = 8$ hours and 1.243 MN/m$^{1.5}$ for $t_h = 16$ hours. At 200°C, K_{IC} decreased to 1.161 MN/m$^{1.5}$ for $t_h = 4$ hours and then recovered to 1.189 MN/m$^{1.5}$ for $t_h = 8$ hours and 1.223 MN/m$^{1.5}$ for $t_h = 16$
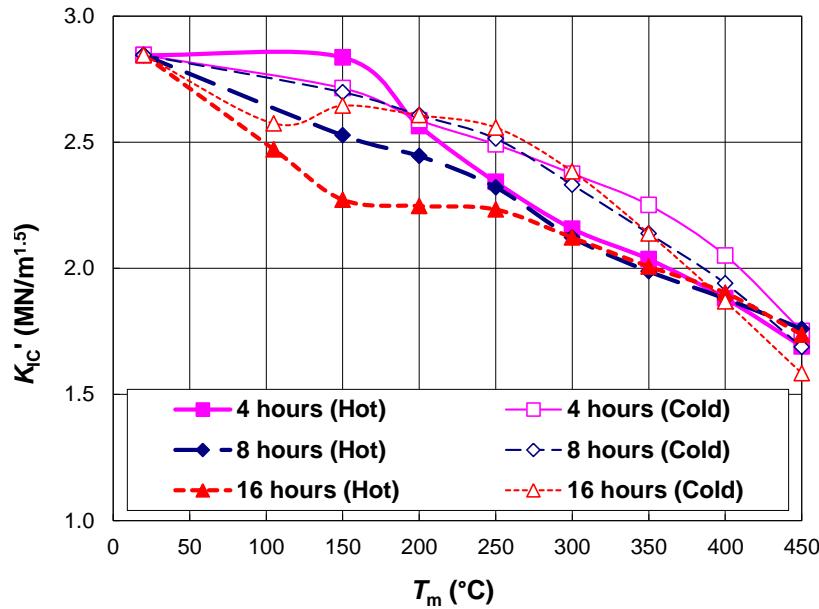
Fig. 5 K_{IC}' versus T_m for different testing conditions and exposure times

hours. At 250ºC, this trend became less obvious. K_{IC} decreased to 1.196 MN/m$^{1.5}$ for t_h = 4 hours and slightly dropped to 1.182 MN/m$^{1.5}$ for t_h = 8 hours and 1.164 MN/m$^{1.5}$ for t_h = 16 hours. The drop in K_{IC} at the early heating stage was caused by the high vapour pressure inside the concrete. At further higher temperatures, K_{IC} continuously and gradually decreased with the exposure time. At 350ºC, K_{IC} dropped to 1.097 MN/m$^{1.5}$ for t_h = 4 hours, 1.039 MN/m$^{1.5}$ for t_h = 8 hours and 1.006 MN/m$^{1.5}$ for t_h = 16 hours. At 450ºC, K_{IC} decreased to 0.942 MN/m$^{1.5}$ for t_h = 4 hours, 0.906 MN/m$^{1.5}$ for t_h = 8 hours and finally 0.866 MN/m$^{1.5}$ for t_h = 16 hours. In this study, the worst case for the hot concrete was recorded for T_m = 450ºC and t_h = 16 hours, and K_{IC} dropped by about 38%.

For the cold concrete, K_{IC} showed different trends with the exposure time at lower heating temperatures up to 200ºC from those at higher heating temperatures. At 150ºC, K_{IC} slightly decreased from 1.389 MN/m$^{1.5}$ before heating to 1.289 MN/m$^{1.5}$ for t_h = 4 hours and then started to recover to 1.297 MN/m$^{1.5}$ for t_h = 8 hours. For t_h = 16 hours, it reached 1.316 MN/m$^{1.5}$. At 200ºC, K_{IC} slightly increased to 1.303 MN/m$^{1.5}$ for t_h = 4 hours but almost unchanged for t_h = 8 hours and slightly decreased to 1.227 MN/m$^{1.5}$ for t_h = 16 hours. At higher heating temperatures, K_{IC} continuously and gradually decreased with the exposure time. At 300ºC, K_{IC} decreased to 1.129 MN/m$^{1.5}$ for t_h = 4 hours, 1.054 MN/m$^{1.5}$ for t_h = 8 hours and 0.996 MN/m$^{1.5}$ for t_h = 16 hours. At 450ºC, K_{IC} dropped to 0.869 MN/m$^{1.5}$ for t_h = 4 hours, 0.812 MN/m$^{1.5}$ for t_h = 8 hours and finally 0.771 MN/m$^{1.5}$ for t_h = 16 hours. In this study, the worst case was recorded for the cold concrete at T_m = 450ºC and t_h = 16 hours with a decrease of about 45% in K_{IC} due to more micro-cracks induced during cooling. In other words, the load capacity in bending indeed decreased during the cooling process for higher heating temperatures.

Fig. 5 shows K_{IC}' at various heating temperatures over three exposure times t_h = 4, 8 and 16 hours for $\dot{T}^+$ = 3°C/min and slow cooling. Similar to K_{IC}, K_{IC}' generally decreased with the increasing hearing temperature and exposure time for both hot and cold concretes.
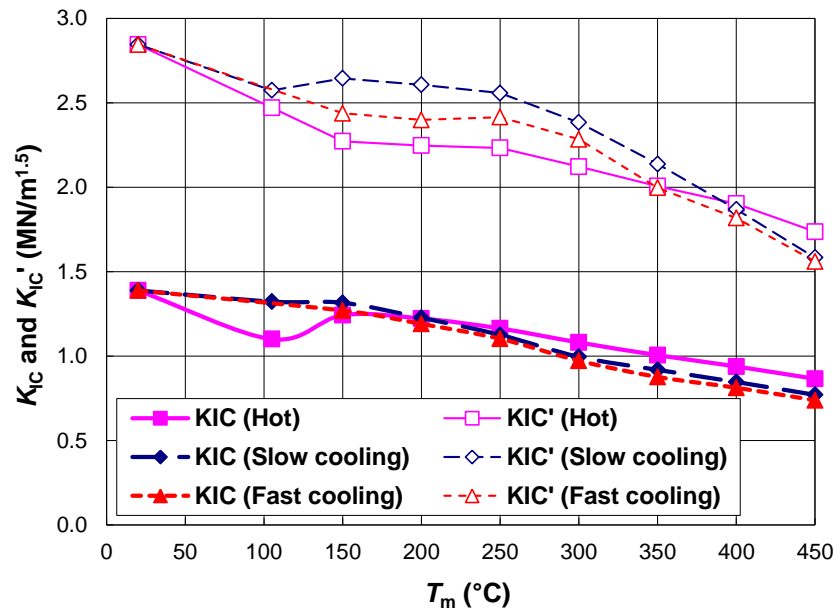
Fig. 6 K_{IC} and K_{IC}' versus T_m for different testing conditions and cooling methods

For the hot concrete at lower heating temperatures up to 250°C, K_{IC}' sustained big variations with t_h. At $T_m = 150$°C, K_{IC}' slightly decreased from 2.845 MN/m$^{1.5}$ before heating ($t_h = 0$) to 2.836 MN/m$^{1.5}$ for $t_h = 4$ hours and then started to decrease quickly to 2.527 MN/m$^{1.5}$ for $t_h = 8$ hours and 2.272 MN/m$^{1.5}$ for $t_h = 16$ hours. At 200°C, K_{IC}' decreased to 2.564 MN/m$^{1.5}$ for $t_h = 4$ hours, 2.445 MN/m$^{1.5}$ for $t_h = 8$ hours and 2.247 MN/m$^{1.5}$ for $t_h = 16$ hours. At 250°C, this trend became less obvious. K_{IC}' decreased to 2.342 MN/m$^{1.5}$ for $t_h = 4$ hours and slightly dropped to 2.321 MN/m$^{1.5}$ for $t_h = 8$ hours and 2.233 MN/m$^{1.5}$ for $t_h = 16$ hours. At further higher temperatures, K_{IC}' continuously and gradually decreased with the exposure time. At 350°C, K_{IC}' dropped to 2.036 MN/m$^{1.5}$ for $t_h = 4$ hours, 1.988 MN/m$^{1.5}$ for $t_h = 8$ hours and slightly to 2.007 MN/m$^{1.5}$ for $t_h = 16$ hours. At 450°C, K_{IC}' decreased to 1.690 MN/m$^{1.5}$ for $t_h = 4$ hours, 1.760 MN/m$^{1.5}$ for $t_h = 8$ hours and finally 1.737 MN/m$^{1.5}$ for $t_h = 16$ hours. In this study, the worst case for the hot concrete was recorded for $T_m = 450$°C and $t_h = 16$ hours, and K_{IC}' decreased by about 39%. The drops in K_{IC}' for the exposure times between 4 and 16 hours at higher heating temperatures were not very large.

For the cold concrete, K_{IC}' showed slightly different trends with the exposure time for lower heating temperatures below 200°C, 200°C to 300°C and higher heating temperatures above 300°C. Below 200°C, a longer exposure time led to a lower K_{IC}'. At 150°C, K_{IC}' decreased from 2.845 MN/m$^{1.5}$ before heating to 2.714 MN/m$^{1.5}$ for $t_h = 4$ hours, 2.698 MN/m$^{1.5}$ for $t_h = 8$ hours and 2.645 MN/m$^{1.5}$ for $t_h = 16$ hours. At 200°C, K_{IC}' was almost the same for different exposure times and were equal to 2.587 MN/m$^{1.5}$ for $t_h = 4$ hours, 2.607 MN/m$^{1.5}$ for $t_h = 8$ hours and 2.607 MN/m$^{1.5}$ for $t_h = 16$ hours, respectively. At 300°C, K_{IC}' decreased to 2.375 MN/m$^{1.5}$ for $t_h = 4$ hours, 2.331 MN/m$^{1.5}$ for $t_h = 8$ hours and 2.384 MN/m$^{1.5}$ for $t_h = 16$ hours. The value of K_{IC}' for $t_h = 16$ hours was slightly higher due to the fact that the fracture energy G_F reached its peak at 300°C. For further higher heating temperatures, K_{IC}' continuously and gradually decreased with the exposure time. At 450°C, K_{IC}' dropped to 1.751 MN/m$^{1.5}$ for $t_h = 4$ hours, 1.688 MN/m$^{1.5}$ for $t_h = 8$ hours and finally 1.584 MN/m$^{1.5}$ for $t_h = 16$ hours. In this study, the worst case was recorded for
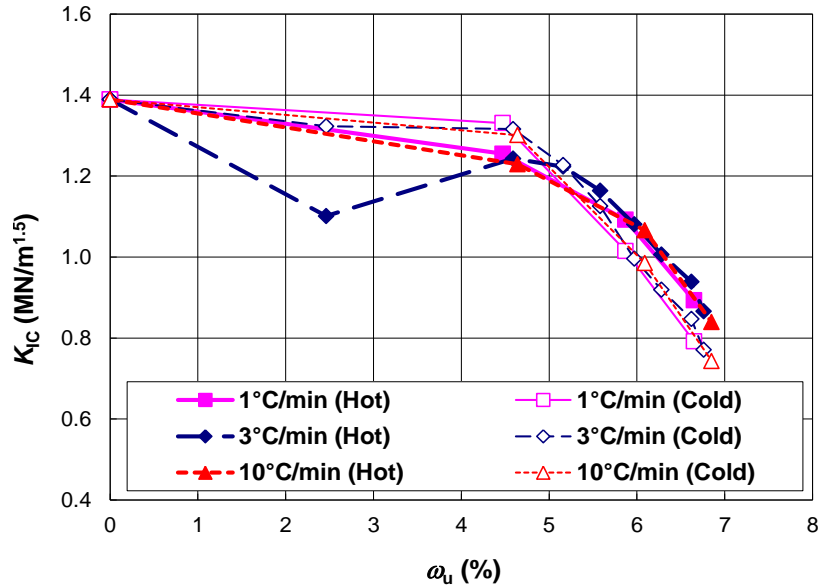
Fig. 7 K_{IC} versus ω_u for different testing conditions at different heating rates

the cold concrete at $T_m = 450°C$ and $t_h = 16$ hours with a decrease of about 44% in K_{IC}'. It is interesting to see that for most heating temperatures, the values of the fracture energy related fracture toughness K_{IC}' for the hot concrete were smaller than those for the cold concrete except 450°C.

4.4 K_{IC} and K_{IC}' versus T_m for different cooling methods

Fig. 6 shows the values of both K_{IC} and K_{IC}' for a fixed exposure time of 16 hours at varied heating temperatures, associated with the heating rate of 3°C/min obtained from the concrete beams which were either slow or fast cooled. The corresponding values for the hot concrete and at room temperature are also plotted in the figure for comparison.

It can be seen that the $K_{IC} - T_m$ curve for fast cooling followed a similar trend to that for slow cooling. For fast cooling at 150°C, K_{IC} slightly decreased from 1.389 MN/m$^{1.5}$ before heating ($t_h = 0$) to 1.270 MN/m$^{1.5}$. At higher temperatures, K_{IC} decreased with the increasing heating temperature. K_{IC} decreased to 1.191 MN/m$^{1.5}$ at 200°C, 0.973 MN/m$^{1.5}$ at 300°C, 0.813 MN/m$^{1.5}$ at 400°C and 0.739 MN/m$^{1.5}$ at 450°C with a final net drop of 47%. For slow cooling. K_{IC} has slightly decreased from 1.389 MN/m$^{1.5}$ before heating ($t_h = 0$) to 1.316 MN/m$^{1.5}$ at 150°C, down by 5%. Thereafter, K_{IC} continuously decreased to 1.126 MN/m$^{1.5}$ at 250°C, 0.996 MN/m$^{1.5}$ at 300°C, 0.847 MN/m$^{1.5}$ at 400°C and 0.771 MN/m$^{1.5}$ at 450°C. The loading capacity for fast cooling was always smaller than that for slow cooling at all heating temperatures, but the difference between two values of K_{IC} for any heating temperature was no more than 0.05 MN/m$^{1.5}$. This means that the cooling rate did influence the behaviour of the concrete at high temperatures to certain degree. Fast cooling always caused slightly more damage to the concrete than slow cooling.

Similarly, the $K_{IC}' - T_m$ curve for fast cooling followed a similar trend to that for slow cooling. For fast cooling at 150°C, K_{IC}' slightly decreased from 2.845 MN/m$^{1.5}$ before heating ($t_h=0$) to 2.438 MN/m$^{1.5}$. At higher temperatures, K_{IC}' decreased with the increasing heating temperature.

K_{IC}' decreased to 2.399 MN/m$^{1.5}$ at 200ºC, 2.284 MN/m$^{1.5}$ at 300ºC, 1.818 MN/m$^{1.5}$ at 400ºC and 1.561 MN/m$^{1.5}$ at 450ºC with a final net drop of 45%. For the slow cooling. K_{IC}' slightly decreased from 2.845 MN/m$^{1.5}$ before heating to 2.645 MN/m$^{1.5}$ at 150ºC, down by 7%. Thereafter, K_{IC}' continuously decreased to 2.558 MN/m$^{1.5}$ at 250ºC, 2.384 MN/m$^{1.5}$ at 300ºC, 1.869 MN/m$^{1.5}$ at 400ºC and 1.584 MN/m$^{1.5}$ at 450ºC. The loading capacity for fast cooling was always smaller than that for slow cooling at all heating temperatures, but the differences between two values at any heating temperature were no more than 0.22 MN/m$^{1.5}$, which are slightly larger than those for K_{IC}.

5. Fracture toughnesses K_{IC} and K_{IC}' versus weight loss ω_u for various heating rates, exposure times and cooling methods

Weight loss ω was also continuously measured to distinguish different stages of the fracture toughness of concrete with heating temperatures. In general, the quick evaporation of capillary water hardly affected the fracture toughness but the evaporation of gel water and chemically bound water and the decomposition significantly decreased the fracture toughness (Zhang *et al.* 2002). Here only the final values of ω, ω_u, for all heating scenarios were used for analysis.

5.1 K_{IC} and K_{IC}' versus ω_u for various $\dot{T}^+$

Fig. 7 shows the K_{IC} versus ω_u relationships for both hot and cold concretes over an exposure time of 16 hours at different heating temperatures for $\dot{T}^+ = 1$, 3 and 10°C/min. The reference classic fracture toughness at room temperature is also plotted in the figure corresponding to zero weight loss. It is obvious that the heating rate influenced the $K_{IC} - \omega_u$ relationships to some degree, but the testing condition incorporating with the heating temperature played a dominating role. K_{IC} for the hot concrete had different trends with ω_u from those for the cold concrete at various $\dot{T}^+$.

For the hot concrete, K_{IC} had a decrease-recovery-decrease tendency with the final weight loss ω_u. In the first two stages, only the test data for $\dot{T}^+ = 3$°C/min were available. In the first stage, K_{IC} sharply decreased with ω_u first from 1.389 MN/m$^{1.5}$ at 20ºC to 1.101 MN/m$^{1.5}$ at 105ºC with a loss of 21%, corresponding to a threshold weight loss $\omega_{u,105} = 2.46\%$. At the second stage, K_{IC} quickly recovered at 150ºC to 1.255, 1.243 and 1.229 MN/m$^{1.5}$ with $\omega_{u,150} = 4.47\%$, 4.59% and 4.64% for $\dot{T}^+ = 1$, 3 and 10°C/min, respectively. Thereafter, K_{IC} continuously decreased with ω_u again. At 300ºC, K_{IC} dropped to 1.092, 1.081 and 1.066 MN/m$^{1.5}$ with $\omega_{u,300} = 5.87\%$, 5.97% and 6.09% for $\dot{T}^+ = 1$, 3 and 10°C/min. Finally at 450ºC, K_{IC} dropped to 0.893, 0.866 and 0.839 MN/m$^{1.5}$ with $\omega_{u,450} = 6.65\%$, 6.76% and 6.85% for $\dot{T}^+ = 1$, 3 and 10°C/min, respectively. This indicates that a higher heating rate slightly decreased K_{IC} and slightly extracted more water from the concrete.

For the cold concrete, K_{IC} sustained two-stage slow decrease – fast decrease tendencies with ω_u for different heating rates. It slowly decreased from 1.389 MN/m$^{1.5}$ at 20ºC with ω_u until 150ºC to 1.331, 1.316 and 1.301 MN/m$^{1.5}$ with $\omega_{u,150} = 4.47\%$, 4.59% and 4.64% for $\dot{T}^+ = 1$, 3 and 10°C/min, respectively. Thereafter K_{IC} decreased with ω_u more quickly and this trend can be expressed by using a bi-linear relationship. At 300ºC, K_{IC} dropped to 1.015, 0.996 and 0.985 MN/m$^{1.5}$ with $\omega_{u,300} = 5.87\%$, 5.97% and 6.09% for $\dot{T}^+ = 1$, 3 and 10°C/min. Finally at 450ºC, K_{IC} dropped to 0.792, 0.771 and 0.743 MN/m$^{1.5}$ with $\omega_{u,450} = 6.65\%$, 6.76% and 6.85% for $\dot{T}^+ = 1$, 3
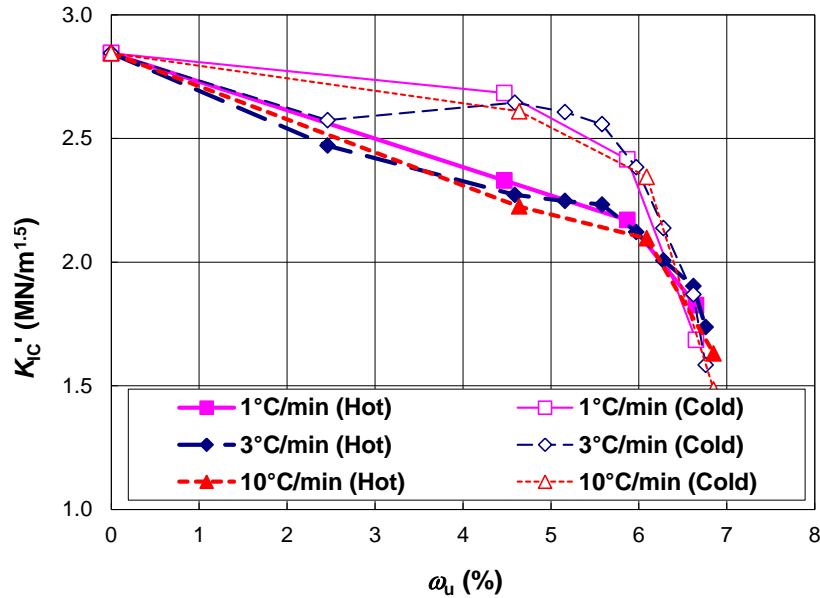
Fig. 8 K_{IC}' versus ω_u for different testing conditions at different heating rates

and 10°C/min, respectively. For $\omega \leq \omega_{u,300}$ corresponding to $T_m \leq 300$°C, the values of K_{IC} for the hot concrete were slightly smaller than those for the cold concrete at the same ω_u. For higher ω_u over $\omega_{u,300}$ or higher heating temperatures over 300°C, the values of K_{IC} for the hot concrete became slightly larger than those for the cold concrete at the same ω_u. Also once again, this indicates that a higher heating rate slightly decreased K_{IC} and slightly increased the weight loss.

Fig. 8 illustrates the K_{IC}' versus ω_u relationships for both hot and cold concretes over an exposure time of 16 hours at different heating temperatures for $\dot{T}^+ = 1$, 3 and 10°C/min. It can be seen that the heating rate influenced the $K_{IC}' - \omega_u$ relationships to certain degree and K_{IC}' for the hot concrete had different trends with ω_u from those for the cold concrete.

For the hot concrete, K_{IC}' had two-stage slow decrease-fast decrease tendencies with the final weight loss ω_u for different heating rates, which can be expressed by using bi-linear relationships. It slowly decreased from 2.845 MN/m$^{1.5}$ at 20°C with ω_u until 150°C to 2.330, 2.272 and 2.225 MN/m$^{1.5}$ with $\omega_{u,150} = 4.47\%$, 4.59% and 4.64% for $\dot{T}^+ = 1$, 3 and 10°C/min, respectively. At 300°C, K_{IC}' dropped to 2.170, 2.122 and 2.096 MN/m$^{1.5}$ with $\omega_{u,300} = 5.87\%$, 5.97% and 6.09% for $\dot{T}^+ = 1$, 3 and 10°C/min. Thereafter K_{IC}' decreased with ω_u more quickly and at 450°C, K_{IC}' dropped to 1.826, 1.737 and 1.631 MN/m$^{1.5}$ with $\omega_{u,450} = 6.65\%$, 6.76% and 6.85% for $\dot{T}^+ = 1$, 3 and 10°C/min, respectively. A higher heating rate slightly decreased K_{IC}' and also slightly extracted more water from the concrete.

For the cold concrete, K_{IC}' also sustained similar two-stage slow decrease-fast decrease tendencies with ω_u for different heating rates except a sudden drop in K_{IC}' at 105°C for $\dot{T}^+ = 3$°C/min. It slowly decreased from 2.845 MN/m$^{1.5}$ at 20°C with ω_u to 2.684, 2.645 and 2.610 MN/m$^{1.5}$ at 150°C with $\omega_{u,150} = 4.47\%$, 4.59% and 4.64% and to 2.415, 2.384 and 2.345 MN/m$^{1.5}$ at 300°C with $\omega_{u,300} = 5.87\%$, 5.97% and 6.09% for $\dot{T}^+ = 1$, 3 and 10°C/min, respectively. Thereafter K_{IC}' rapidly decreased with ω_u and dropped to 1.686, 1.584 and 1.485 MN/m$^{1.5}$ at 450°C with $\omega_{u,450}$
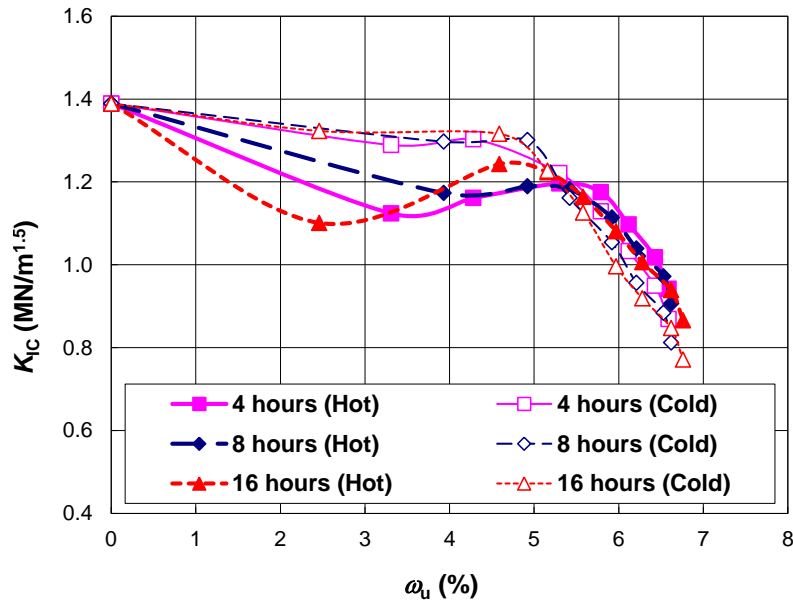
Fig. 9 K_{IC} versus ω_u for different testing conditions and exposure times

= 6.65%, 6.76% and 6.85% for $\dot{T}^+$ = 1, 3 and 10°C/min. For $\omega \leq \omega_{u,300}$ corresponding to T_m = 300ºC, the values of K_{IC}' for the hot concrete were much smaller than those for the cold concrete at the same ω_u at different heating rates. For the higher weight loss $\omega_{u,450}$ or higher heating temperature 450ºC, the corresponding values of K_{IC}' for the hot concrete were slightly larger than those for the cold concrete at the same ω_u. Once again, a higher heating rate slightly decreased K_{IC}' and slightly increased the weight loss.

5.2 K_{IC} and K_{IC}' versus ω_u for various t_h

Fig. 9 shows K_{IC} versus ω_u relationships for both hot and cold concretes at various heating temperatures over three exposure times, i.e., t_h = 4, 8 and 16 hours, at $\dot{T}^+$ = 3°C/min. It can be seen that K_{IC} generally decreased with ω_u for both hot and cold concretes over various exposure times but followed different trends.

For the hot concrete, K_{IC} sustained three-stage decrease-recovery-decrease tendencies over three different exposure times. In the first stage, it sharply decreased with ω_u until its minimum values were reached. The corresponding weight loss was very much dependent on the exposure time and was equal to 3.31% for t_h = 4 hours at T_m = 150°C, 3.93% for t_h = 8 hours at 150°C and 2.46% for t_h = 16 hours at 105°C. The corresponding values of K_{IC} were 1.124, 1.173 and 1.101 MN/m$^{1.5}$ with net drops of 19%, 16% and 21% respectively compared with the room temperature value 1.389 MN/m$^{1.5}$. The first two weight loss values corresponded to T_m = 150°C but the third one to T_m = 105°C due to no available data for t_h = 4 and 8 hours at 105°C. In the second stage, K_{IC} continuously increased with ω_u until another peak was reached. At the peak K_{IC} was equal to 1.196 MN/m$^{1.5}$ for t_h = 4 hours, 1.189 MN/m$^{1.5}$ for t_h = 8 hours but 1.243 MN/m$^{1.5}$ for t_h = 16 hours with the corresponding weight loss of 5.30% at 250ºC, 4.92% at 200ºC and 4.59% at 150ºC. The peak shifted towards left with the increasing exposure time but the peak value seemed accordingly to
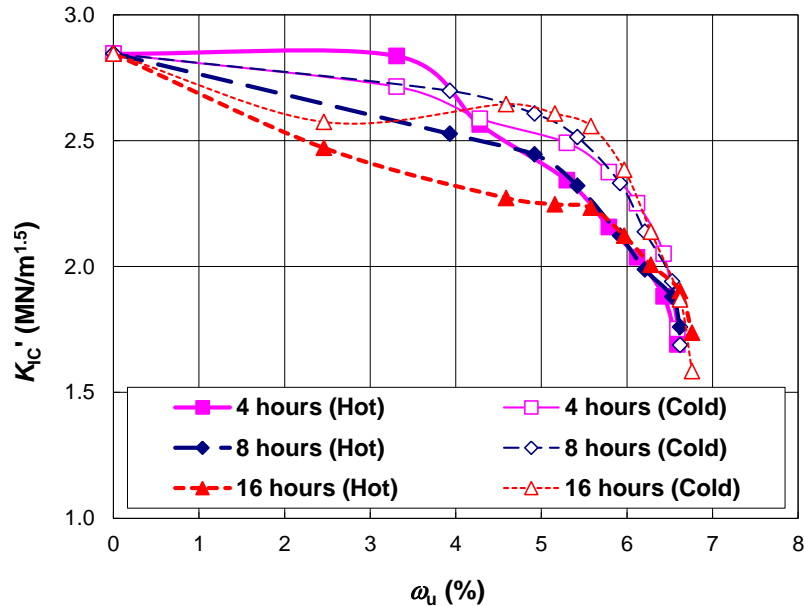
Fig. 10 K_{IC}' versus ω_u for different testing conditions and exposure times

slightly increase. For a given weight loss in this stage, however, a longer exposure time led to a higher K_{IC}. In the third stage, K_{IC} continuously decreased with the increasing ω_u. At $T_m = 450°C$, K_{IC} decreased to 0.942, 0.906 and 0.866 MN/m$^{1.5}$ for $t_h = 4$, 8 and 16 hours, with net drops of 32%, 35% and 38%, corresponding to $\omega_{u,450} = 6.59\%$, 6.62% and 6.76%, respectively. Three $K_{IC} - \omega_u$ curves in this stage were quite parallel and a longer exposure time now led to a lower K_{IC} and also a lightly larger ω_u for the same heating temperature.

For the cold concrete, K_{IC} sustained two-stage slow decrease – fast decrease tendencies with ω_u for varied exposure times. In the first stage, K_{IC} only slightly decreased with ω_u until certain weight loss was reached. The values of the characteristic weight loss largely depended on the exposure time t_h and were equal to 4.28% for $t_h = 4$ hours at 200°C, 4.92% for $t_h = 8$ hours at 200°C and 4.59% for $t_h = 16$ hours at 150°C, and the corresponding K_{IC} values were 1.303, 1.301 and 1.316 MN/m$^{1.5}$, with net drops of 6%, 6% and 5% respectively. In the second stage, K_{IC} continuously decreased with ω_u. At $T_m = 450°C$, K_{IC} decreased to 0.869, 0.812 and 0.771 MN/m$^{1.5}$ for $t_h = 4$, 8 and 16 hours respectively, with net drops of 37%, 42% and 45%, corresponding to $\omega_{u,450} = 6.59\%$, 6.62% and 6.76%. Similarly, three $K_{IC} - \omega_u$ curves in this stage were quite parallel and a longer exposure time led to a lower K_{IC} and also a slightly larger ω_u for the same heating temperature.

Fig. 10 shows K_{IC}' at various heating temperatures over three exposure times $t_h = 4$, 8 and 16 hours for $\dot{T}^+ = 3°C/min$. Similar to K_{IC}, K_{IC}' generally decreased with the increasing hearing temperature and exposure time for both hot and cold concretes but followed different trends.

For the hot concrete over three different exposure times, K_{IC}' generally sustained two-stage slow decrease-fast decrease tendencies. In the first stage, it slowly decreased with ω_u until some threshold values were reached, largely depending on exposure time, which were equal to 3.31% for $t_h = 4$ hours at 150°C, 4.92% for $t_h = 8$ hours at $T_m = 200°C$ and 5.58% for $t_h = 16$ hours at 250°C. The corresponding K_{IC}' values were 2.836, 2.445 and 2.233 MN/m$^{1.5}$ with net drops of
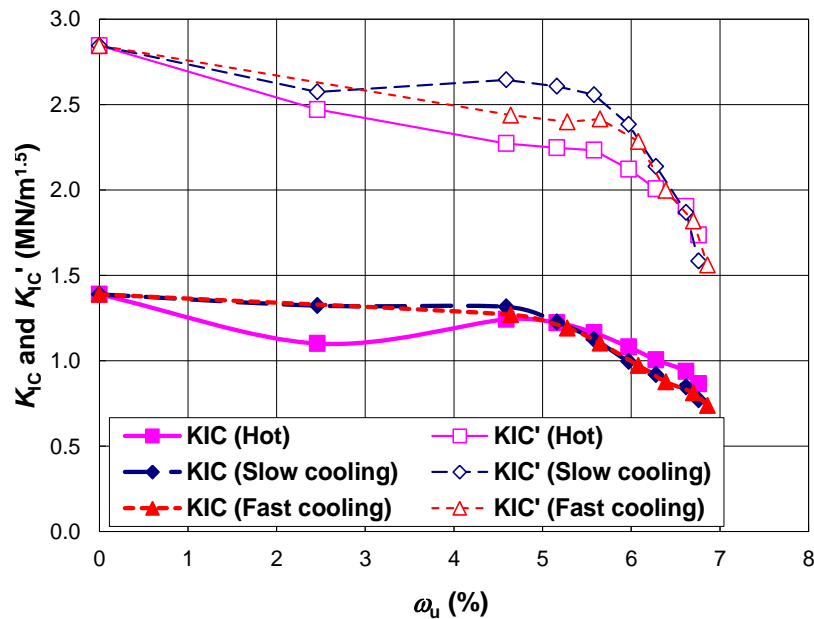
Fig. 11 K_{IC} and K_{IC}' versus ω_u for different testing conditions and cooling methods

0.3%, 14% and 22% respectively compared with the room temperature value 2.845 MN/m$^{1.5}$. The threshold values shifted towards right with the increasing exposure time and largely decreased. It can also be seen that the decreasing rate for K_{IC}' in this stage also largely increased with the increasing ω_u. In the second stage, K_{IC}' continuously decreased with the increasing ω_u. At $T_m =$ 450°C, K_{IC}' decreased to 1.690, 1.760 and 1.737 MN/m$^{1.5}$ for $t_h =$ 4, 8 and 16 hours, with net drops of 41%, 38% and 39%, corresponding to $\omega_{u,450} =$ 6.59%, 6.62% and 6.76%, respectively. Three $K_{IC}' - \omega_u$ curves in this stage almost coincided and a longer exposure time did not largely influence K_{IC}' except lightly leading to a larger ω_u for the same heating temperature.

For the cold concrete, K_{IC}' sustained similar two-stage slow decrease-fast decrease tendencies with ω_u for varied exposure times. In the first stage, K_{IC}' only slightly decreased with ω_u until some threshold values for weight loss at $T_m =$ 250°C were reached, which were equal to 5.30% for $t_h =$ 4 hours, 5.42% for $t_h =$ 8 hours and 5.58% for $t_h =$ 16 hours. The corresponding K_{IC}' values were 2.491, 2.514 and 2.558 MN/m$^{1.5}$, with net drops of only 12%, 12% and 10%, but slightly higher for longer exposure times. In the second stage, K_{IC}' continuously decreased with ω_u more rapidly. Similarly, three $K_{IC}' - \omega_u$ curves in this stage were quite parallel and a longer exposure time led to a lower K_{IC}' and also a slightly larger ω_u for the same heating temperature. At $T_m =$ 450°C, K_{IC}' decreased to 1.751, 1.688 and 1.584 MN/m$^{1.5}$ for $t_h =$ 4, 8 and 16 hours, with net drops of 38%, 41% and 44%, corresponding to $\omega_{u,450} =$ 6.59%, 6.62% and 6.76%, respectively. Figure 10 also indicates that the $K_{IC}' - \omega_u$ curves for the hot concrete are generally lower than those for the cold concrete for all exposure times except the K_{IC}' value for $t_h =$ 4 hours at $T_m =$ 150°C which was larger for the hot concrete.

5.3 K_{IC} and K_{IC}' versus ω_u for different cooling methods

Fig. 11 shows both K_{IC} and K_{IC}' versus ω_u relationships for a fixed exposure time of 16 hours at
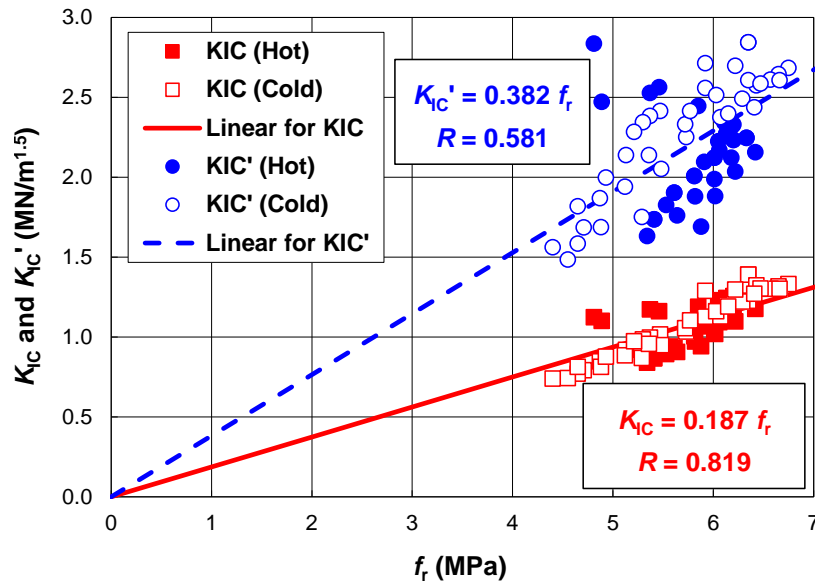
Fig. 12 K_{IC} and K_{IC}' versus f_r for the complete test series and testing conditions

varied heating temperatures, associated with the heating rate of 3°C/min obtained from the concrete beams which were either slow or fast cooled after having been heated. The corresponding relationships for the hot concrete are also plotted in the figure for comparison.

For the $K_{IC} - \omega_u$ relationships, both slow and fast cooled concretes sustained similar two-stage slow decrease-fast decrease tendencies. K_{IC} first slowly decreased with ω_u until $T_m = 150$°C corresponding to $\omega_{u,150} = 4.59\%$ and $K_{IC} = 1.316$ MN/m$^{1.5}$ for the slow cooled concrete and $\omega_{u,150} = 4.64\%$ and $K_{IC} = 1.270$ MN/m$^{1.5}$ for the fast cooled concrete. Thereafter, K_{IC} decreased with ω_u more rapidly until $T_m = 450$°C corresponding to $\omega_{u,450} = 6.76\%$ and $K_{IC} = 0.771$ MN/m$^{1.5}$ for the slow cooled concrete and $\omega_{u,450} = 6.86\%$ and $K_{IC} = 0.739$ MN/m$^{1.5}$ for the fast cooled concrete. For all heating temperatures, a faster cooling led to a slightly lower K_{IC} and a slightly larger ω_u. In contrast, the K_{IC} values for the hot concrete were lower than those for the concretes cooled in either ways when $\omega \leq \omega_{u,150}$ but became larger when $\omega > \omega_{u,150}$.

For the $K_{IC}' - \omega_u$ relationships, both slow and fast cooled concretes also sustained similar two-stage slow decrease-fast decrease tendencies. K_{IC}' first slowly decreased with ω_u until $T_m = 250$°C corresponding to $\omega_{u,250} = 5.58\%$ and $K_{IC}' = 2.558$ MN/m$^{1.5}$ for the slow cooled concrete and $\omega_{u,250} = 5.65\%$ and $K_{IC}' = 2.415$ MN/m$^{1.5}$ for the fast cooled concrete. Thereafter, K_{IC}' decreased with ω_u more rapidly until $T_m = 450$°C corresponding to $\omega_{u,450} = 6.76\%$ and $K_{IC}' = 1.584$ MN/m$^{1.5}$ for the slow cooled concrete and $\omega_{u,450} = 6.86\%$ and $K_{IC}' = 1.561$ MN/m$^{1.5}$ for the fast cooled concrete. For all heating temperatures, a faster cooling led to a relatively lower K_{IC}' and a slightly larger ω_u. In contrast, the K_{IC}' values for the hot concrete were lower than those for the concretes cooled in either ways when $T_m \leq 350$°C but became larger when $T_m > 350$°C.

6. Fracture toughnesses K_{IC} and K_{IC}' versus the modulus of rupture f_r

Fig. 12 illustrates a relationship between K_{IC} and f_r for the complete test series, including all

heating scenarios and testing conditions. It can be seen that all the test results can be represented by a linear equation as

$$K_{IC} = 0.187 \, f_r \quad \text{or} \qquad K_{IC} = 0.749 \, \sigma_N \qquad (9)$$

with a linear correlation coefficient $R = 0.819$. This relationship can also be directly confirmed from Eq. (1). In comparison with Eq. (1), the term $\sqrt{a} \, F(\alpha)$ can be obtained as 0.749 $m^{0.5}$. This means that for a given material and geometry, the classic fracture toughness K_{IC} can be fully connected to and determined by the modulus of rupture of the notched beam. It should be mentioned that the obtained empirical constants in Eq. (9) are only valid for the concrete beams with $H = 100$ mm and $a_0/H = 0.5$.

A similar equation can also be derived for the relationship between the fracture energy related fracture toughness, K_{IC}', and the modulus of rupture, f_r, by using linear regression on the test results as

$$K_{IC}' = 0.382 \, f_r \quad \text{or} \qquad K_{IC}' = 1.528 \, \sigma_N \qquad (10)$$

with a linear correlation coefficient $R = 0.581$. The linear equation and test results for the K_{IC}' versus f_r relationship are also illustrated in Fig. 12. Because K_{IC}' depends not only on the maximum load and geometric configurations, but also on the failure displacement and the Young's modulus, a bigger scatter together with a lower R value can be expected.

7. Conclusions

In this study, the classic fracture toughness K_{IC} of high performance concrete, together with the fracture energy related fracture toughness K_{IC}', was evaluated by conducting three-point bending tests on a total of 240 notched beams at various heating temperatures up to 450°C (hot) and in slow or fast cooled-down states (cold). The heating rate varied from 1°C/min, 3°C/min up to 10°C/min, and the exposure time varied from 4 hours, 8 hours up to 16 hours. The weight loss ω as a very important physical parameter was continuously monitored during the complete heating, exposure, testing and cooling process. The following conclusions can be drawn accordingly.

• Among the investigated influencing parameters, heating temperature, exposure time and testing temperature were still primary factors on both K_{IC} and K_{IC}'.

• K_{IC} generally decreased with the increasing heating temperature for the hot concrete but sustained a two-stage slow decrease-fast decrease tendency for the cold concrete. K_{IC}' for the hot concrete sustained a three-stage fast decrease-slow decrease-fast decrease tendency but a two-stage slow decrease-fast decrease tendency for the cold concrete. Below 250°C, the K_{IC} values for the hot concrete were lower than those for the cold concrete, while at higher heating temperatures the K_{IC} values for the cold concrete became larger. For the fracture energy related fracture toughness, K_{IC}', this transiting temperature was about 400°C.

• Heating rate was a secondary influencing factor on K_{IC} and K_{IC}' for both hot and cold concretes. A higher heating rate would only slightly decrease both K_{IC} and K_{IC}'. However, a very high heating rate would cause spalling for the high performance concrete at high heating temperatures.

• A longer exposure time would lead to a larger K_{IC} at lower heating temperatures but to a lower K_{IC} at higher heating temperatures for both hot and cold concretes. However, a longer

exposure time would always lead to a lower K_{IC}' for all heating temperatures.

• Cooling methods adopted in this study seemed to be a secondary influencing factor on K_{IC} and K_{IC}' for both hot and cold concretes. K_{IC} only slightly decreased for the fast cooling at all heating temperatures, while the decreased amplitudes for K_{IC}' were larger at all heating temperatures.

• The weight loss as a continuous non-reversible process monotonically increased with the increasing heating temperature and largely influenced the fracture toughness parameters K_{IC} and K_{IC}'. Higher heating temperatures incorporating with longer exposure times would always lead to larger weight losses but hygric equilibrium states could be reached if exposure time would be long enough. A higher heating rate would slightly increase the weight loss. The fast cooling would also cause higher weight loss than the slow cooling. The $K_{IC} - \omega_u$ and $K_{IC}' - \omega_u$ relationships for different heating rates, exposure times and cooling methods were extensively assessed.

• Fairly linear relationships between the classic fracture toughness K_{IC} or the fracture energy related fracture toughness K_{IC}' and the modulus of rupture f_r existed for the test results on both hot and cold concretes at all heating scenarios in this study.

Acknowledgments

References

Bažant, Z.P. (1984), "Size effect in blunt fracture: Concrete rock and metal", *ASCE J. Eng. Mech.*, **110**(4), 518-535.

Bažant, Z.P. and Oh, B.H. (1983), "Crack band theory for fracture of concrete", *RILEM Mater. Struct.*, **16**(93), 155-177.

Bažant, Z.P., Kim, J.K. and Pfeiffer, P.A. (1986), "Nonlinear fracture properties from size effect tests", *ASCE J. Struct. Eng.*, **112**(2), 289-307.

Dong, W., Wu, Z. and Zhou, X. (2013), "On fracture process zone and crack extension resistance of concrete based on initial fracture toughness", *Constr. Build. Mater.*, **49**(12), 352-363.

Dong, W., Wu, Z., Zhou, X. and Wang, C. (2016), "A comparative study on two stress intensity factor-based criteria for prediction of mode-I crack propagation in concrete", *Eng. Fract. Mech.*, **158**, 39-58.

Gettu, R., Bažant, Z.P. and Karr, M.E. (1990), "Fracture properties and brittleness of high-strength concrete", *ACI Mater. J.*, **87**(6), 608-618.

Hamoush, S.A., Abdel-Fattah, H. and McGinley, M.W. (1998), "Residual fracture toughness of concrete exposed to elevated temperature", *ACI Mater. J.*, **95**(6), 689-694.

Hillerborg, A., Modeer, M. and Petersson, P.E. (1976), "Analysis of crack formation and crack growth in concrete by means of fracture mechanics and finite elements", *Cement Concrete Res.*, **6**(6), 773-782.

Ince, R. (2010), "Determination of concrete fracture parameters based on two-parameter and size effect models using split-tension cubes", *Eng. Fract. Mech.*, **77**, 2233-2250.

Kaplan, M.F. (1961), "Crack propagation and the fracture of concrete", *ACI J.*, **58**(5), 591-610.

Karihaloo, B.L. and Nallathambi, P. (1989), "An improved effective crack model for the determination of fracture toughness of concrete", *Cement Concrete Res.*, **19**, 603-610.

Nallathambi, P., Karihaloo, B.L. and Heaton, B.S. (1984), "Effect of specimen and crack sizes, water/cement ratio and coarse aggregate texture upon fracture toughness of concrete", *M. Concrete Res.*, **36**(129), 227-236.

Phillips, D.V. and Zhang, B. (1993), "Direct tension tests on notched and un-notched plain concrete

specimens", *M. Concrete Res.*, **45**, 25-35.

Prokoski, G. (1995), "Fracture toughness of concrete at high temperature", *J. Mater. Sci.*, **30**, 1609-1612.

RILEM Technical Committee 89 FME (1990a), "Draft recommendation: Determination of fracture parameters (K_{IC}^s and CTOD$_c$) of plain concrete using three-point bend tests", *RILEM Mater. Struct.*, **23**, 457-460.

RILEM Technical Committee 89 FME (1990b), "Draft recommendation: Size-effect method for determining fracture energy and process zone size of concrete", *RILEM Mater. Struct.*, **23**, 461-465.

Shah, S.P. (1990), "Experimental methods for determining fracture process zone and fracture parameters", *Eng. Fract. Mech.*, **35**(1/2/3), 3-14.

Wu, Z., Rong, H., Zheng, J. and Dong, W. (2013), "A numerical method for mixed I-II crack propagation in concrete", *ASCE J. Eng. Mech.*, **139**(11), 1530-1538.

Wu, Z., Rong, H., Zheng, J., Xu, F. and Dong, W. (2011), "An experimental investigation on the FPZ properties in concrete using digital image correlation technique", *Eng. Fract. Mech.*, **78**(17), 2978-2990.

Xu, S. and Reinhardt, H.W. (1999a), "Determination of double-K criterion for crack propagation in quasi-brittle materials. Part I: Experimental investigation of crack propagation", *J. Fract.*, **98**, 111-149.

Xu, S. and Reinhardt, H.W. (1999b), "Determination of double-K criterion for crack propagation in quasi-brittle materials. Part II: Analytical evaluating and practical measuring methods for three-point bending notched beams", *J. Fract.*, **98**, 151-177.

Xu, S. and Reinhardt, H.W. (1999c), "Determination of double-K criterion for crack propagation in quasi-brittle materials. Part III: Compact tension specimens and wedge splitting specimens", *J. Fract.*, **98**, 179-193.

Xu, S. and Reinhardt, H.W. (2000), "A simplified method for determining double-K fracture parameters for three-point bending tests", *J. Fract.*, **104**, 181-209.

Yu, K. and Lu, Z. (2014), "Determining residual double-K fracture toughness of post-fire concrete using analytical and weight function method", *Mater. Struct.*, **47**(5), 839-852.

Zhang, B. (2011), "Effects of moisture evaporation (weight loss) on fracture properties of high performance concrete subjected to high temperatures", *Fire Safety J.*, **46**, 543-549.

Zhang, B. and Bićanić, N. (2002) "Residual fracture toughness of normal- and high-strength gravel concrete after heating to 600°C", *ACI Mater. J.*, **99**(3), 217-226.

Zhang, B., Bićanić, N., Pearce, C.J. and Balabanic, G. (2000), "Residual fracture properties of normal- and high-strength concrete subject to elevated temperatures", *M. Concrete Res.*, **52**(2), 123-136.

Zhang, B., Bićanić, N., Pearce, C.J. and Phillips, D.V. (2002) "Relationship between brittleness and moisture loss of concrete exposed to high temperatures", *Cement Concrete Res.*, **32**, 363-371.

Zhang, B., Cullen, M. and Kilpatrick, T. (2014) "Fracture toughness of high performance concrete subjected to elevated temperatures Part 1 The effects of heating temperatures and testing conditions (hot and cold)", *Adv. Concrete Constr.*, **2**(2), 145-162.

Zhang, B., Cullen, M. and Kilpatrick, T. (2016), "Spalling of heated high performance concrete due to thermal and hygric gradients", *Adv. Concrete Constr.*, **4**(1), 1-14.

CC